Check for updates

Morphology and thermal properties of poly(L-lactic acid) nucleated with 2,2′-(butane-1,4-diylbis(oxy))di(benzohydrazide)†

Safaa H. El-Taweel, [ID] *[ab] Sherif M. H. Sanad [ID] [a] and Ahmed E. M. Mekky [ID] [a]

This study evaluates the modification of biodegradable poly(L-lactide) (PLLA) using a novel organic nucleating agent, 2,2′-(butane-1,4-diylbis(oxy))di(benzohydrazide) (BDOBH) with a low concentration range from (0.3–3 wt%). The novelty of this work lies in the development and application of BDOBH as a highly efficient, low-loading organic nucleator tailored to improve PLLA's crystallization behavior and thermal properties—key limitations in its broader industrial use. The evaluation is conducted through differential scanning calorimetry (DSC), thermogravimetric analysis (TGA), Fourier-transform infrared spectroscopy (FTIR), and polarized optical microscopy. FTIR analysis reveals the presence of H-bonding interaction between BDOBH and PLLA. DSC results significantly improve PLLA's crystallization rate, with BDOBH in a concentration range from 0.3 to 0.7 wt%. The total crystallinity of PLLA increases from 12% to 56–60% without a change in PLA's crystallography; moreover, the maximum temperature of the cold crystallization peak shifts to a lower value by 35 °C after incorporating BDOBH-0.7 into PLLA. POM results reveal a drastic decrease in the spherulitic size of PLLA. Furthermore, the presence of BDOBH enhances the thermal stability of PLLA. The nonisothermal cold crystallization behavior of PLLA nucleated by BDOBH is evaluated using the modified Avrami and Mo models. Multiple indicators of nonisothermal crystallization, including the crystallization half-time and crystallization rate constant, indicate that BDOBH greatly expedites the crystallization process. The activation energy values of the plain PLLA and PLLA-BDOBH, as computed using the Kissinger–Akahira–Sunose (KAS) model, decrease when BDOBH is incorporated. These findings highlight BDOBH's potential as a cost-effective and scalable additive to tailor PLLA crystallization, supporting its use in environmentally friendly packaging, biomedical devices, and other high-performance biodegradable applications.

1. Introduction

Polylactic acid (PLLA) is a biodegradable and bio-derived polymer extensively employed in packaging, textiles, and biomedical hardware[1–3] PLLA's comparatively slow crystallization rate significantly impacts the material's mechanical properties, thermal resilience, and overall efficacy. The slow crystallization rate leads to a prolonged processing cycle, poor heat resistance, and an amorphous state even after processing. In response to this problem, scientists have investigated the application of nucleating chemicals, which accelerate the crystallization rate by offering active sites for crystal development.

It has been demonstrated that one of the best ways to improve PLLA's crystallization capacity is to add appropriate

[a]Chemistry Department, Faculty of Science, Cairo University, Orman-Giza, 12613, Egypt. E-mail: Safaaeltaweel@cu.edu.eg; shamdi@sci.cu.edu.eg

[b]Engineering and Materials Science Department, German University in Cairo, New Cairo City, Egypt

nucleating agents.[4,5] Inorganic fillers like talc,[6,7] TiO$_2$,[8,9] graphene oxide,[10–12] and carbon nanotubes,[13,14] as well as low-molecular-weight organic substances,[15,16] including hydrazides,[16,17] esters, amides,[18] cyanuric acid, and orotic acid[15] have been chosen to initiate the crystallization of PLLA. The main criteria for nucleating agents are their ability to disperse evenly in PLLA, function efficiently at low concentrations, and significantly accelerate the crystallization process. Regarding inorganic additions, organic chemicals tend to distribute more evenly in the PLLA matrix due to their solubility in PLLA melt.[16]

Some amides have been reported as highly effective nucleating agents for PLLA. Li *et al.*[19] found that *N*-aminophthalimide could accelerate the crystallization of PLLA. Recently, Nakajima *et al.*[18] used 1,3,5-benzenetricarboxyamide derivatives to enhance the crystallization of PLLA successfully. Even more recently, Bai *et al.*[20] demonstrated that one of the above derivatives, *i.e.*, *N*,*N*′,*N*′-tricyclohexyl-1,3,5-benzenetricarboxyamide (TMC-328) could be used to control the superstructure of PLLA effectively. In a study conducted by Song *et al.*[21] and Xu *et al.*[22] The crystallization behavior and nucleation ability of PLLA nucleated by TMC were examined in the low

concentration range from 0.25 to 1.0. The findings indicated that even a small amount of TMC significantly impacted the promotion of PLLA nucleation.

The efficacy of hydrazides as nucleating agents for PLLA has been examined in several studies.[23–28] The introduction of hydrazide units into the PLLA matrix functions as a heterogeneous nucleation site, decreasing the activation energy necessary for crystallization and consequently expediting the crystallization process. These improvements in crystallization result in enhanced thermal characteristics, including higher heat resistance and improved dimensional stability throughout processing.

Kawamoto et al.[27] synthesized a range of hydrazide derivatives and identified octamethylene dicarboxylic dibenzoylhydrazide (OMBH) with 1 wt% as the most effective for accelerating PLLA crystallization at higher cooling rates. Xing et al.[29] further confirmed that OMBH is an efficient nucleating agent for PLLA, noting that it reduced the spherulitic size and increased the crystallinity of the nucleated PLLA with 0.5 wt%. Suttiruengwong et al.[30] reported that adding 0.5 wt% of N,N'-ethylenebis(10-undecenamide) (EBU) or tetramethylenedicarboxylic dibenzoylhydrazide (TMC-308) significantly increased the crystallinity of PLLA. Xue et al.[23] reported that adding 0.05 wt% of TMC significantly reduced the crystallization halftime of PLLA.

A study by Liu et al.[25] found that the addition of N',N',N',N'-salicylic tetra(1,2,4,5-benzenetetracarboxylic acid) hydrazide (BAS) in the range from 0.5 to 3 wt% to PLLA can enhance its thermal stability and fluidity but reduce its light transmittance. Cai et al.[31] showed the most significant improvement in the crystallization process when incorporating 1.5 wt% of the salicyloyl hydrazide derivative.

The addition of N-(benzoyl)stearic acid hydrazide significantly improved the tensile strength, modulus, and elongation at the break of PLLA, as was reported by Cai and Li.[32] The nucleation efficiency of hydrazide compounds is attributed to the dipole–dipole interaction between the nucleating agent's imino group and the PLLA molecular carbonyl group.[15] A benzene ring on some hydrazide nucleating agents promotes the nucleation of PLLA.[33]

To the best of our knowledge, the evaluation of 2,2'-(butane-1,4-diylbis(oxy))di(benzohydrazide) (BDOBH) (Scheme 1) as a novel nucleating agent for PLLA has not been reported so far. The physical and mechanical characteristics, as well as the performance of PLLA, are significantly influenced by their crystallization behavior. Our work mainly aimed to assess the crystallization kinetics of PLLA-BDOBH using nonisothermal cold crystallization studies. The experimental data was analyzed

using many models, specifically the modified Avrami and Mo models. Analysis of the effective activation energy for non-isothermal crystallization processes was conducted using the Kissinger–Akahira–Sunose (KAS) method.

PLLA-BDOBH's morphology was examined using polarized light optical microscopy. This work investigated the impact of BDOBH on the thermal stability of PLLA using thermogravimetric analysis (TGA).

2. Experimental part

2.1 Materials

The PLLA (Biomer L9000) polymer, which has a melt flow index of 3 g/10 min (2.16 kg, 190 °C), was obtained from the Biomer Products Factory in Germany. The compound had a weight-average molecular weight of 2×10^5 g mol^{-1} and a poly-dispersity index 2. The synthesis of 2,2'-(butane-1,4-diylbis(oxy))di(benzohydrazide) (BDOBH) was carried out as described in ref. 34. Comprehensive information on the synthesis and characterization of 2,2'-(butane-1,4-diylbis(oxy)) di(benzohydrazide) is present in a ESI.†

2.2 Preparation of PLLA-BDOBH

The casting film technique prepared mixtures of PLLA with different concentrations of BDOBH. Firstly, the desired mass of BDOBH powder was combined with dimethylformamide at a ratio (1 : 10) and stirred at 60 °C for 30 min. A suitable mass of PLLA was dissolved in chloroform in a ratio (1 : 50). The PLLA/ chloroform and BDOBH/DMF solutions were combined and stirred for 2 h. As a consequence of this process, the solvent was evaporated at room temperature for 2 weeks to obtain a uniform film. The produced cast films were subjected to drying in a vacuum oven at 70 °C for 6 h. Subsequently, these blends were melted between hot melt presses at 200 °C for 2 min. A series of PLLA-BDOBH-x blends, each containing different weight percentages of BDOBH (0.0, 0.3, 0.7, 1.0, and 3.0), were investigated here.

2.3 Characterization PLLA-BDOBH

TGA was used to investigate the thermal stability of PLLA, BDOBH, and PLLA-BDOBH using a Shimadzu TGA-50H thermal analyzer. The samples were heated at 10 °C min^{-1} from 50 °C to 500 °C in a nitrogen environment.

FTIR spectra were recorded on a Smart iTR, an ultra-high-performance, versatile attenuated total reflectance (ATR) sampling accessory for the Nicolet iS10 FT-IR spectrometer.

Spherulite morphology of plain PLLA and BDOBH-nucleated PLLA was examined using a polarized optical microscope (POM), Imager A1, equipped with a digital camera system, Axiocam, from Carl Zeiss AG, Germany. A thin film of each PLLA-BDOBH was placed between two glass slides. The material was melted in an oven set at 200 °C for 2 min and then promptly moved to another oven set at 125 °C for 2 h of isothermal crystallization.

Wide-angle X-ray diffraction (WAXRD) was performed on a Bruker D8 advance diffractometer (Bruker, Germany) set to 40
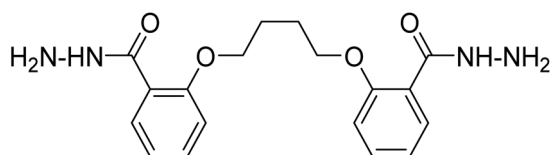
Scheme 1 Structure of BDOBH.

kV and 40 mA. Measurements utilized CuKα radiation with a wavelength of 0.15418 nm, and the scan was carried out at a rate of 0.05° min⁻¹.

The DSC studies were conducted in aluminum pans using a DSC-TA-Q100 analytical apparatus from TA instrument, USA, in a nitrogen atmosphere. The equipment underwent calibration using meticulously pure indium and sapphire standards. Each sample, weighing approximately 6 mg, was utilized. Three distinct thermal programs were utilized, each with different considerations.

In program A, the PLLA-BDOBH-x was initially heated to 200 °C at a rate of 10 °C min⁻¹ and then maintained at that temperature for 3 min to eliminate any prior thermal effects. Next, the samples were cooled to 30 °C at a rate of 10 °C min⁻¹ and then reheated to 200 °C at the same rate to determine the thermal characteristics (*i.e.*, melt crystallization temperature T_c, glass transition temperature T_g, cold crystallization temperature T_{cc}, and melting temperature T_m). In order to quantify the extent of the crystalline phase present in the sample, one can compute the crystallinity (X_c) according to eqn (1):

$$X_{crys} = \frac{\Delta H_{PLLA-BDOBH}}{(1 - f_{BDOBH})\Delta H_{PLA}^{100\% \text{ crystalline}}} \times 100 \qquad (1)$$

$\Delta H_{PLLA-BDOBH}$ is melting enthalpy of PLLA-BDOBH and $\Delta H_{PLLA}^{100\% \text{ crystalline}}$ is the enthalpy of 100% crystalline PLLA, 93.6 J g⁻¹,[35] f_{BDOBH} is the BDOBH fraction (*i.e.*, 0.3 wt%).

Program B, the PLLA-BDOBH were annealed at 90 °C for 3 min, then cooled to room 30 °C at a cooling rate of 5 °C min⁻¹ and reheated to 190 °C at a heating rate of 10 °C min⁻¹. Program C involved heating the PLLA-BDOBH-x to 190 °C for 3 min, then cooling them to 30 °C at a cooling rate of 40 °C min⁻¹, and then heating them at various heating rates of 3, 4, 5, and 6 °C min⁻¹ for nonisothermal cold crystallization. The nonisothermal crystallization kinetics characteristics, such as the modified Avrami rate constant and effective activation energy, were estimated using the cold crystallization peaks at various heating rates.

3. Results and discussion

3.1 Thermal stability

TGA was used to assess the thermal stability of plain PLLA, BDOBH, and PLLA-BDOBH. Fig. 1 displays the TGA curves obtained at a 10 °C min⁻¹ rate under N₂ conditions. Fig. 1 provides evidence of a single thermal deterioration stage for the examined samples, indicating good compatibility of PLLA and BDOBH. Table 1 provides the temperatures corresponding to different levels of mass loss. These include the temperatures for 10% mass loss ($T_{10\%}$), 90% mass loss ($T_{90\%}$), and the maximum mass loss rate (T_{max}). The data presented in Table 1 demonstrates that $T_{10\%}$ and T_{max} values slightly increase when BDOBH is added to PLLA. The movement of PLLA chains is hindered, which in turn slows down the thermal deterioration of the PLLA
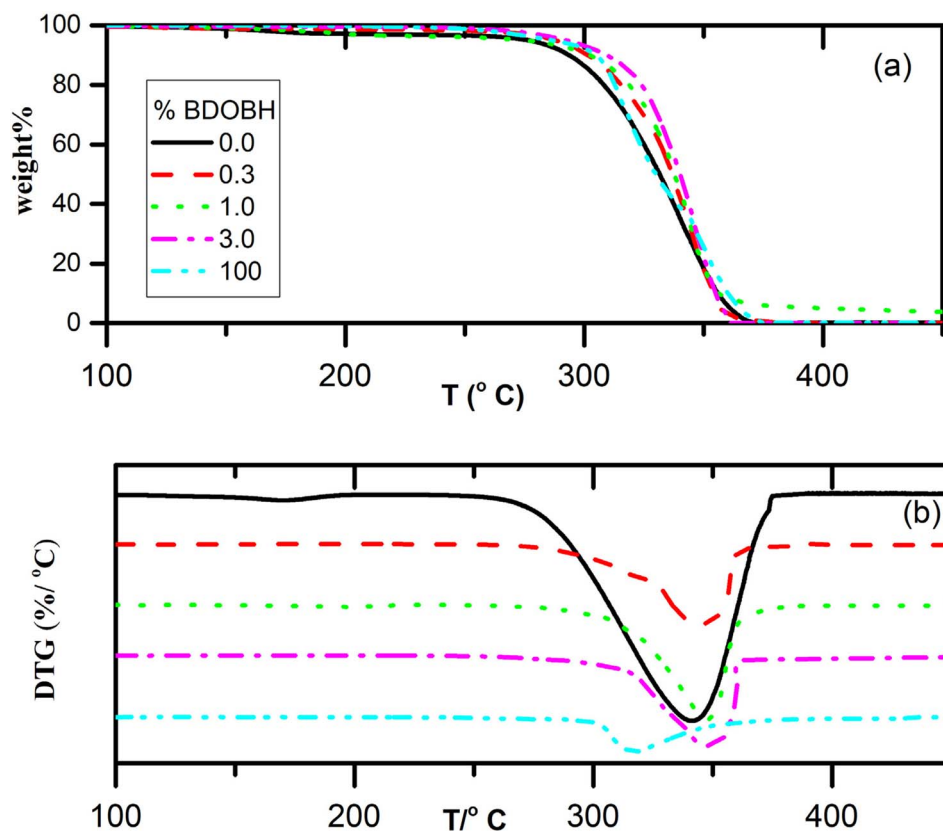

Fig. 1 TGA (a) and DTGA (b) for PLLA, BDOBH, and PLLA-BDOBH.

Table 1   TGA parameters for PLLA and BDOBH and PLLA–BDOBH

Sample	$T_{10\%}$ (°C)	$T_{max\ PLLA}$ (°C)	$T_{90\%}$ (°C)
PLLA	276	341	356
PLLA-BDOBH-0.3	301	347	355
PLLA-BDOBH-1.0	303	348	355
PLLA-BDOBH-3.0	309	350	355
BDOBH	305	318	360

samples due to the interface interaction between PLLA and BDOBH particles (*i.e.*, the presence of hydrogen bonds)[15,36,37] and the enlarged crystalline areas.[28] This result indicates that BDOBH improves the thermal stability of PLLA and can widen the processing temperature. BDOBH likely has a decomposition temperature close to or higher than that of PLLA, meaning its addition does not introduce early degradation pathways that would significantly shift the TGA profile. Moreover, BDOBH is present at relatively low weight percentages (≤3%), and its influence on the overall thermal decomposition process is minimal. The bulk degradation mechanism of PLLA, primarily driven by random chain scission and ester bond cleavage, remains dominant.[38] In addition, BDOBH may be well-dispersed within the PLLA matrix without forming thermally unstable domains, preventing the occurrence of secondary degradation effects. A similar trend was observed for PLLA with *N,N,N,N′*-salicylic tetra(1,2,4,5-benzenetetracarboxylic acid) hydrazide,[23] salicylic hydrazide derivative,[25] *N,N′*-bis(salicyloyl) *p*-phthalic acid dihydrazide,[39] PLLA/*N,N,N′*-tris(benzoyl)trimesic acid hydrazide (TTAD),[40] and (0.5–3 wt%) of *N,N′*-bis(phenyl) 1,4-naphthalenedicarboxylic acid dihydrazide (NAPH).[41]

3.2   FTIR analysis

Fig. 2 shows the FTIR spectroscopic images of PLLA-BDOBH. The FTIR spectrum of BDOBH showed absorption bands at 3230 and 3072 cm^{-1} owing to NH and NH$_2$ stretching, in addition to two bands at 1556 and 1365 cm^{-1} due to NH bending and C–N stretching vibrations, respectively. The spectrum revealed two bands at 3037 and 748 cm^{-1} due to sp^2–C–H stretching and bending vibrations of typical *ortho*-disubstituted benzenes, in addition to three bands at 2933, 2881, and 1454 cm^{-1} owing to symmetric, asymmetric sp^3–C–H stretching and CH$_2$ bending. Moreover, it showed two bands at 1650 and 1295 cm^{-1} corresponding to carbonyl stretching and bending vibrations and two bands at 1602 and 1486 cm^{-1} corresponding to aromatic C=C stretching vibrations. Also, it showed four bands at 1247, 1193, 1149, and 1080 cm^{-1} owing to different C–O stretching and CH$_2$ rocking or wagging bending vibrations.

On the other hand, the FTIR spectrum of PLLA showed absorption bands at 3664 and 3503 cm^{-1} due to dissociative and associative OH stretching.[42,43] These bands represent several terminal OH and COOH functions found in PLLA chains. The spectrum revealed two bands at 2997 and 2933 cm^{-1} due to sp^3–C–H stretching.[44] Moreover, it showed an absorption band at 1749 cm^{-1} corresponding to the carbonyl stretching vibration.[42,44] The C–C stretching bands at 867 and
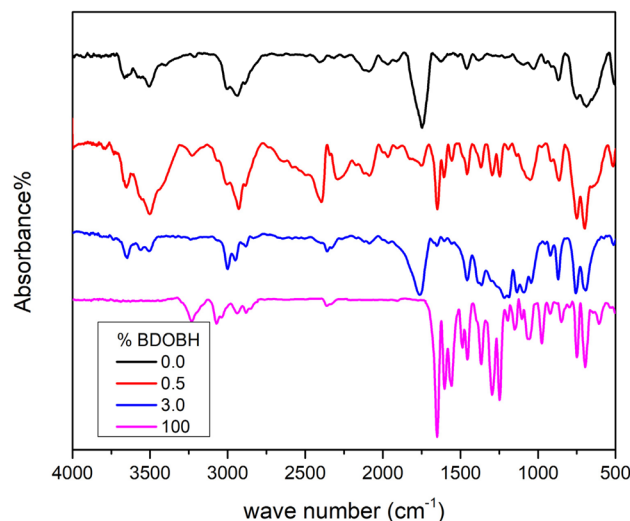

Fig. 2   FTIR spectra of PLLA-BDOBH.

748 cm^{-1} are related to the degree of PLLA crystallization, where the intensity of the prior bands is related to the amorphous and crystalline phases, respectively.[45,46]

The FTIR spectrum of BDOBH-0.3 showed a red shift in the frequency of the absorption bands due to two OH groups, in addition to the carbonyl function. The absorption bands due to these groups appeared at 3650, 3499, and 1746 cm^{-1}, respectively. The H-bonding between BDOBH and PLLA chains could explain this behavior. Moreover, the spectrum showed weak absorption bands at 3226, 3062, and 1648 cm^{-1}. These bands are due to the NH and CO groups found in BDOBH. Again, these bands appeared at a lower frequency when compared with the absorption bands of BDOBH-100. The presence of BDOBH characteristic absorption bands in BDOBH-0.3 confirms the incorporation of BDOBH into the chains of PLLA. The intensity of C–C stretching bands of BDOBH-0.3 at 862 and 750 cm^{-1} reflects the improvement in the degree of PLLA crystallization obtained. The spectrum showed an intense absorption band at 750 cm^{-1} and a weak band at 862 cm^{-1} compared to BDOBH-0.

On the other hand, the FTIR spectrum of BDOBH-3.0 showed a blue shift in the frequency of the absorption bands due to the carbonyl functions in both PLLA and BDOBH. The absorption bands due to these groups appeared at 1759 and 1752 cm^{-1}, respectively. This behavior could be explained by the large amount of agglomeration of BDOBH at this concentration. Moreover, the spectrum showed two bands at 869 and 756 cm^{-1} of comparable intensity, reflecting the decrease in the PLLA crystallization obtained in the BDOBH-3.0 blend.

3.3   The crystal of PLLA-BDOBH

Fig. 3 presents the XRD patterns of crystallized PLA and PLA-BDOBH after annealed at 125 °C for 2 hours. All PLA samples display a prominent diffraction peak at $2\theta = 16.8°$, corresponding to the (110) and/or (200) planes, along with a less intense peak around 19°, which is associated with the (203) reflection plane. The diffraction patterns of PLA-BDOBH closely
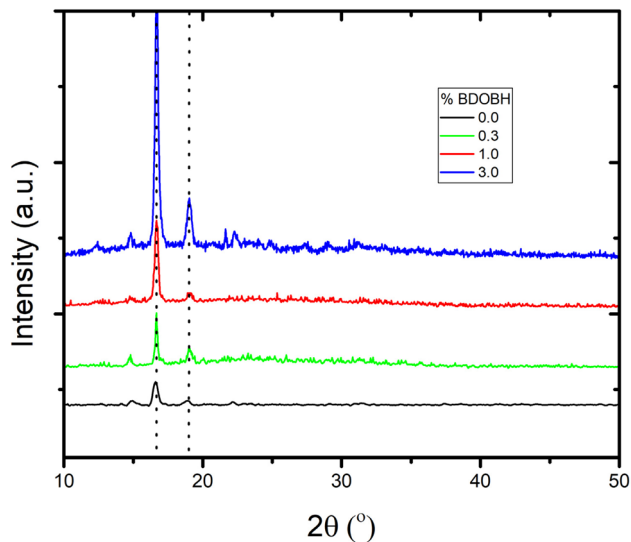
Fig. 3 XRD patterns of the PLA-BDOBH.

resemble those of neat PLA, suggesting that the addition of BDOBH does not alter the crystalline structure of PLA. Similar trend has been observed for PLLA with hydrazide.[23]

3.4 Morphology of PLLA-BDOBH

The POM micrographs of PLLA with varying BDOBH concentrations obtained at 125 °C during isothermal crystallization are displayed in Fig. 4. As anticipated, plain PLLA exhibits a typical spherulitic morphology (Fig. 4). However, depending on the composition of BDOBH, the morphology of nucleated PLLA differs greatly from that of plain PLLA. For instance, when the

concentration of BDOBH is in the range of 0.3–0.7, the nucleation density rises significantly.

As the concentration of BDOBH is 1 to 3.0%, a large number of tiny spherulites change into a small number of large-size spherulites with a large amount of agglomeration of BDOBH. This result reflects that the solubility of BDOBH in PLLA decreases with the increase in its content from 1 to 3.0%.

One can conclude that good solubility can be achieved from 0.3 to 0.7% in the concentration range. A similar conclusion has been drawn for PLLA/TMC-328,[47] PLLA/a self-assembly aryl amide[48] PLLA/MOF,[35,49] PLLA/tetramethylenedicarboxylic di-(2-hydroxybenzohydrazide) (TMBH)[26] PLLA/dilithium hexahydrophthalate,[50] PLLA/multi amide.[22]

3.5 DSC measurements

Fig. 5 illustrates a comparative analysis of the melt crystallization behavior of plain PLLA and PLLA-BDOBH at a cooling rate of 10 °C min^{-1}. Samples of PLLA containing BDOBH in the range of 0.3–0.7% show obvious crystallization peaks in contrast with PLLA, PLLA/BDOBH-1.0, and PLLA/BDOBH-3.0. This result shows that a small concentration range is beneficial for the nucleation and crystallization of PLLA.

Incorporating BDOBH into the PLLA matrix facilitates dipole–dipole interaction between the imino and the carbonyl groups of the PLLA.[15,21,22] The dipole–dipole interaction and the formation of a hydrogen bond with the carbonyl group of PLLA facilitate the nucleating efficiency of BDOBH within the PLLA melt matrix and reduce PLLA's nucleation-free energy, as shown in FTIR analysis.

A limited concentration of BDOBH is due to a large amount of aggregation of BDOBH into PLLA, as discussed in the POM section. A similar phenomenon has been observed in the system of PLLA/octamethylenedicarboxylic dibenzoyl hydrazide (TMC-
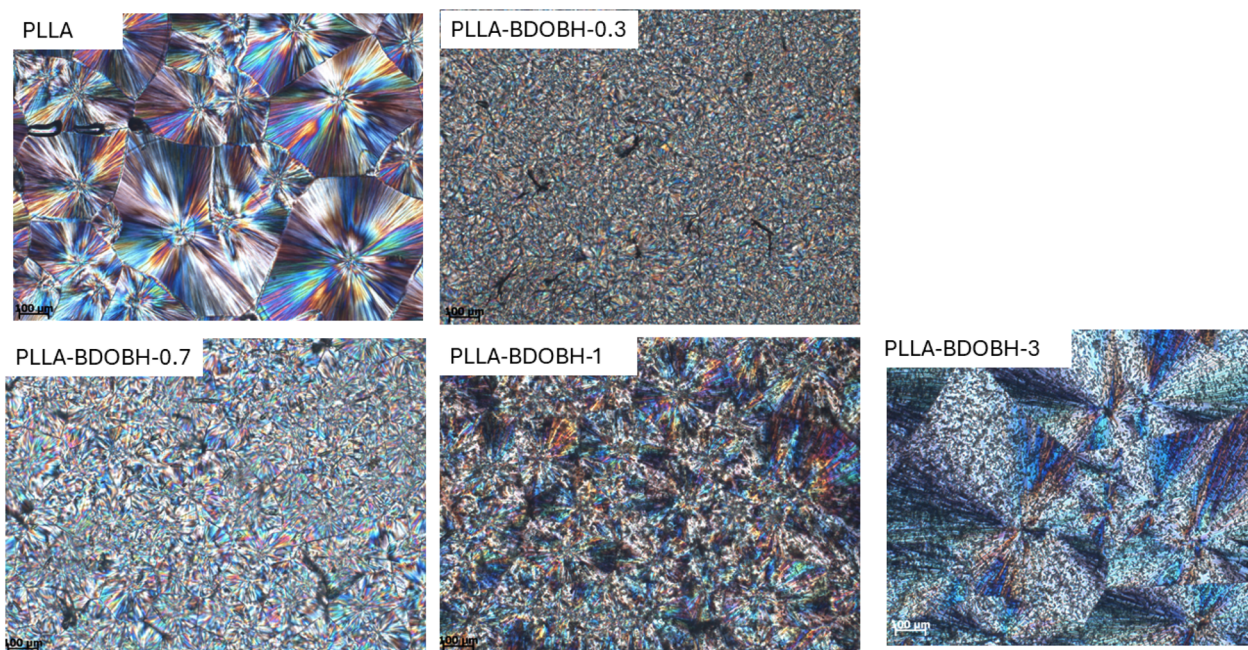

Fig. 4 Polarized optical micrographs for PLLA–BDOBH at a crystallized temperature of 125 °C.
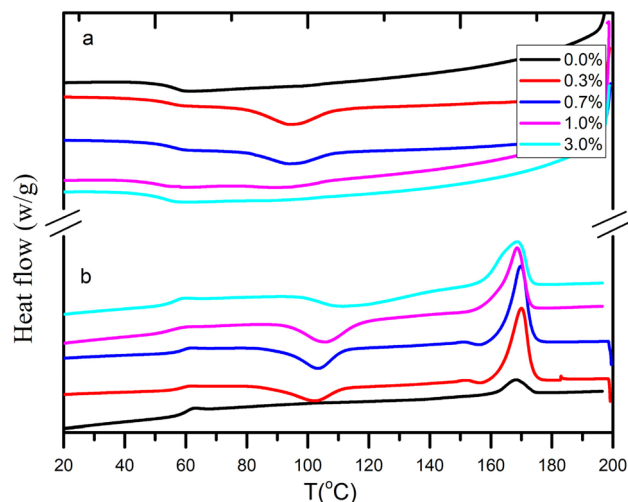
Fig. 5 DSC thermograms of PLLA and PLLA-BDOBH at (a) a cooling rate of 10 °C min^{-1} from 190; (b) a heating rate of 10 °C min^{-1} from 20 °C.

300) and tetramethylenedicarboxylic dibenzoyl hydrazide (TMC-308) PLLA/MOF.[35,49]

In the case of plain PLLA, there is no discernible crystallization peak during the cooling scan of 10 °C min^{-1}. Instead, cold crystallization occurs at around 137 °C, with a minor crystallization enthalpy (ΔH_{cc}) of around 4 J g^{-1} during the subsequent heating run of 10 °C min^{-1}, as shown in Fig. 5b. During the second heating run, homogeneous nuclei of PLLA and heterogeneous nuclei of BDOBH coexist above the glass transition temperature, accelerating the cold crystallization process of PLLA-BDOBH.

It is well known that as the cold crystallization peak (T_{cc}) value shifted to a lower temperature value, the polymer became more accessible for crystallization. Fig. 5b shows that sharp cold crystallization peaks with lower temperature maxima were observed for PLLA-BDOHB in the concentration range from 0.3 to 1.0 wt% and weak, broad crystallization peaks for plain PLLA and PLLA-BDOBH-3.0. This may be attributed to the poor crystallinity of PLLA and a large aggregation of BDOBH into PLLA, as discussed in the POM section. The ΔH_{cc} value of cold crystallization in PLLA-BDOBH blends was significantly higher than that in plain PLLA, reflecting that the crystallinity of PLLA-BDOBH during this heat treatment is much higher.

Consequently, the relative crystallinities (X_c) of PLLA-BDOBH samples are also much higher than that of plain PLLA, which indicates better nucleating efficiency and faster overall crystallization. It is well known that the melting process strongly depends on the crystallization process and heating rate. A weak, broad melting peak was observed in plain PLLA. The melting peak of PLLA drastically changed into a more intense and narrower melting peak, with a considerable melting enthalpy value upon incorporating BDOBH, as shown in Fig. 5b and Table 2. The melting peak became broader when BDOBH concentration was increased from 1.0% to 3.0%. It is worth mentioning that the total crystallinity percentage is significantly changed from 12% for plain PLLA to 56–60% for PLLA-BDOBH, as shown in Table 2. DSC results reflect the accelerating and nucleation role of BDOBH for PLLA crystallization. Previous studies[15] have documented that the overall crystallinity of PLLA increases to around 55% when various hydrazide chemicals are used.

Various factors influence the crystallization behavior, including additives such as nucleating agents and plasticizers and processing conditions like the cooling rate and final melting temperature. This is a widely recognized phenomenon in the field of crystallization research. As previously mentioned, the introduction of BDOBH significantly impacted the crystallization of PLLA when the cooling rate was set at 10 °C min^{-1}. The influence of a cooling rate on the crystallization behavior of PLLA-BDOBH samples was investigated using DSC at a cooling rate of 5 °C min^{-1}, as depicted in Fig. 6.

As a heterogeneous organic nucleating agent, BDOBH can decrease the surface free energy of nucleation, which in turn enhances the formation of PLLA nuclei (as discussed in the POM section). This phenomenon results in the sharpening of the melt crystallization peak and, consequently, an increase in its melt crystallization enthalpy when BDOBH is incorporated in the concentration range from 0.3 to 0.7%, as presented in Fig. 6.

3.6 Nonisothermal cold crystallization kinetics

Fig. 7 presents the DSC thermograms of plain PLLA and PLLA-BDOBH after a second heating scan at varying heating rates. Exothermic cold crystallization peaks were detected at temperatures ranging from 104 °C to 110 °C for plain PLLA, 99 °C to 106 °C for PLLA-BDOBH-0.3, 96 °C to 102 °C for PLLA-BDOBH-0.7, and 98 °C to 105 °C for PLLA-BDOBH-1.0.

When BDOBH was incorporated into the PLLA matrix, a distinct, sharper, narrower cold crystallization peak occurred during the heating scan, as shown in Fig. 7. The heating rate significantly influenced the enthalpy of cold crystallization for plain PLLA, as shown in Table 3. The enthalpy of cold crystallization for PLLA-BDOBH slightly depended on the heating scan, as indicated in Table 3. The relative crystallinity $X(T)$ as a function of crystallization temperature T was driven from

Table 2 Thermal transitions of PLLA-BDOBH from DSC thermograms with cooling and heating rates of 10 °C min^{-1}

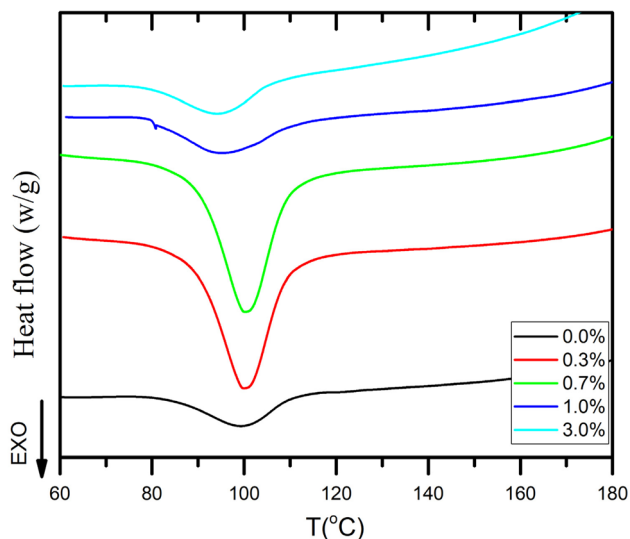| BDOBH (wt%)	T_c (°C)	ΔH_c (J g^{-1})	T_g (°C)	ΔC_p	T_{cc} (°C)	ΔH_{cc} (J g^{-1})	T_m (°C)	ΔH_m (J g^{-1})	X_c (%)
0.0	—	—	59	0.62	137	4	168	11	12
0.3	94	17	58	0.4	102	23	170	52	56
0.7	94	10	58	0.46	104	27	170	53	60
1.0	95	5	55	0.65	106	32	169	48	52
3.0	—	—	55	0.68	113	32	168	47	52

Fig. 6 Melt crystallization Peak of PLLA-BDOBH from 190 °C at a cooling rate of 5 °C min^{-1}.
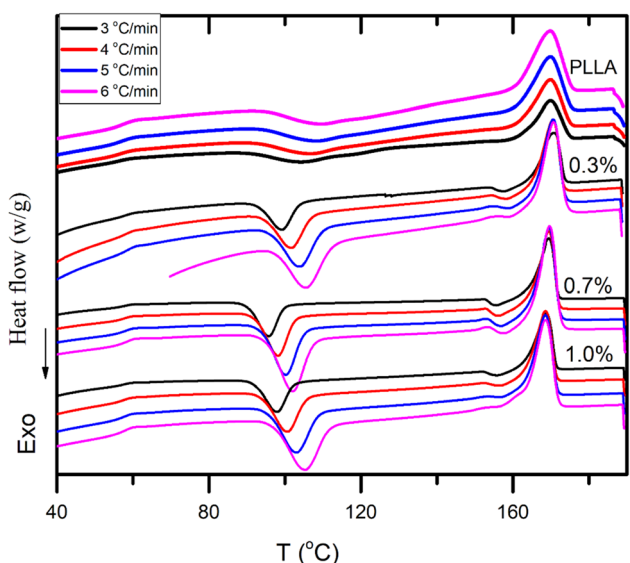

Fig. 7 Non-isothermal DSC different heating curves of plain PLLA and PLLA-BDOBH.

Fig. 7. A formulation for the relative crystallinity $X(T)$ as a function of crystallization temperature T in the non-isothermal crystallization process is:

$$X(T) = \frac{\int_{T_0}^{T} \left(\frac{\partial H}{\partial t}\right) \partial t}{\int_{T_0}^{T_\infty} \left(\frac{\partial H}{\partial t}\right) \partial t} \qquad (2)$$

Assuming that T_0, T, and T_∞ represent the starting, arbitrary, and final crystallization temperatures, ∂H is the enthalpy of the cold crystallization that occurs within an infinitesimal temperature range ∂T. The conversion of crystallization temperature

(T) to crystallization time (t) can be achieved by applying the following eqn (3):

$$t = \frac{|T - T_0|}{\varphi} \qquad (3)$$

Let φ denote the heating rate.

Fig. 8 illustrates the plots of the relative degree of crystallinity $X(T)$ and $X(t)$ *versus* the crystallization temperature (T) and time t, respectively, at various heating rates. All $X(T)$–T and $X(t)$–t curves displayed sigmoidal curves, where a longer crystallization time was seen with the lowest heating rate. A higher heating rate leads to a higher crystallization temperature at the same relative crystallinity, as shown in Fig. 8a and Table 3. The relative crystallization gradually reaches 1 with increasing temperature for a given heating rate, as illustrated in Fig. 8a. The PLLA-BDOBH's crystallization started and finished at lower temperatures than that of plain PLLA, indicating the nucleation efficiency of BDOBH. The $t_{0.5}$ and $t_{0.9}$, which are the time required to reach 50 and 90% of the relative degree of crystallinity, were evaluated from Fig. 8a and listed in Table 3. $t_{0.5}$ and $t_{0.9}$ decrease with increasing heating rate, as shown in Fig. 8b. The $t_{0.5}$ of plain PLLA was found to be longer than that of PLLA-BDOBH samples when subjected to the same heating rate. This observation indicates that adding BDOBH accelerated PLLA's crystallization rate. The values of $t_{0.5}$ PLLA-BDOBH-1 and PLLA-BDOBH-3 were greater than those of PLLA-BDOBH-0.3 and PLLA-BDOBH-0.7 due to solubility limit and agglomeration in parallel with POM and DSC results.

Jeziorny's modified Avrami equation[51] can be employed to analyze the non-isothermal cold crystallization kinetics of PLLA-BDOBH.[8,52–56]

$$\log[-\ln(1 - X(t))] = \log k_t + n \log(t) \qquad (4)$$

where $X(t)$ represents the relative crystallinity at time t.

The Avrami exponent and crystallization rate constant are n and k_t respectively. Because temperature fluctuates constantly during non-isothermal crystallization, the constants k_t and n have physical meanings different from those of isothermal crystallization. According to Jeziorny's proposal, k_t needs to be modified by the heating rate as follows:

$$k_c = \frac{\log k_t}{\varphi} \qquad (5)$$

Fig. 9 shows the modified Avrami plot for plain PLLA and PLLA-BDOBH samples for $X(t)$ in the range of 0.2 to 0.8. The values of R^2 are 0.999, indicating that modified Avrami describes the experimental nonisothermal data well. For all PLLA samples in Table 3, k_c shifted to a higher value as the heating rate increased. The k_c value of plain PLLA was slower than that of nucleated PLLA-BDOBH. This suggests that adding a BDOBH enhanced the nonisothermal crystallization of PLLA. The mean n value for plain PLLA was 2.32, and for nucleated PLLA-BDOBH, it was 3, respectively. Aht-Ong *et al.* reported a homogeneous nucleation of neat PLLA with circular disk

Table 3 Modified Avrami parameters for PLLA/BDOBH

| PLLA-BDOBH	φ (°C min^{-1})	T_c (°C)	ΔH_c (J g^{-1})	X_c	n	$\log Z_t$	$Z_c \times 10^{-2}$ (min^{-1})	$t_{0.5}$ (min)	$t_{0.9}$ (min)	R^2
0.0	3	105	35	37	2.4	−1.7	26.7	5.6	9.9	0.999
	4	107	30	32	2.3	−1.5	41.6	4.1	7.6	0.999
	5	109	27	29	2.2	−1.2	56.9	3.1	5.9	0.999
	6	110	25	27	2.1	−1.0	67.9	2.5	5.0	0.999
0.3	3	99	38	41	2.9	−1.3	37.9	2.4	3.5	0.998
	4	102	38	41	2.8	−0.96	57.7	2.0	2.9	0.998
	5	104	38	41	2.9	−0.89	66.5	1.8	2.6	0.998
	6	106	36	39	2.7	−0.59	79.8	1.5	2.2	0.998
0.7	3	96	38	41	3.1	−1.3	36.1	2.4	3.7	0.999
	4	98	38	41	3.0	−0.98	56.9	1.9	2.8	0.999
	5	100	38	41	3.0	−0.79	69.3	1.6	2.0	0.999
	6	102	40	43	3.0	−0.67	77.0	1.5	2.3	0.999
1.0	3	98	40	43	3.1	−1.4	34.6	2.9	4.4	0.999
	4	101	40	43	2.9	−1	54.8	2.1	3.3	0.999
	5	103	40	43	2.9	−0.9	66.6	1.8	2.9	0.999
	6	105	39	45	2.9	−0.7	75.2	1.7	2.7	0.999
3.0	3	99	40	44	2.1	−1.5	32.9	4	7	0.999
	4	101	40	44	2.0	−1.1	52.0	3.1	5.8	0.999
	5	103	38	41	1.9	−0.93	65.2	2.5	5.1	0.999
	6	106	36	40	1.8	−0.79	73.9	2.2	4.2	0.999
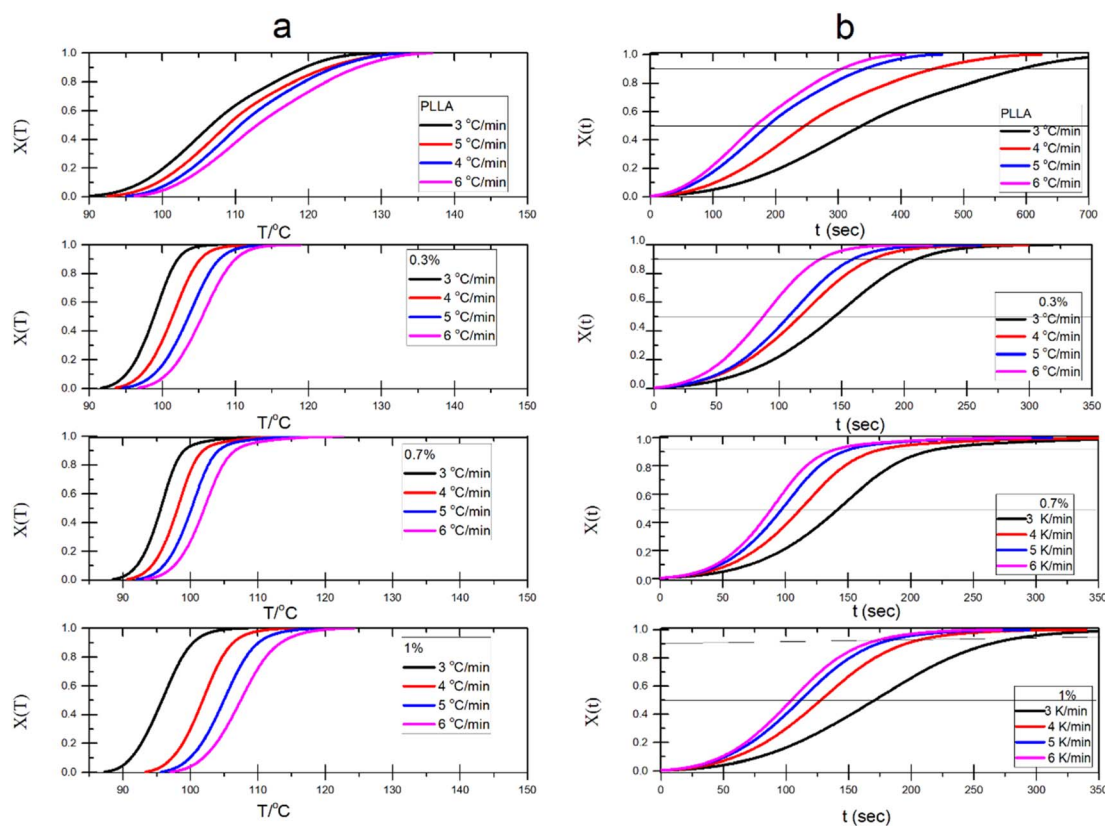
Fig. 8 Relative crystallinity as a function of; (a) crystallization temperature, (b) crystallization time of plain PLLA and PLLA–BDOBH.

shape growth for $n = 2$.[57] For $n = 3$, it suggests that heterogeneous nucleation with spherical growth could be observed.[57] These findings suggested that incorporating BDOBH altered the chain folding crystallization mechanism of PLLA, which led to an increase in n values.

It is worth noting that the Avrami n value and the crystallization rate of PLLA-BDOBH-3 are very close to those of neat PLLA (see Table 3), as also seen in the corresponding crystallization curves (Fig. 7). This further supports the interpretation that 3 wt% BDOBH does not significantly accelerate
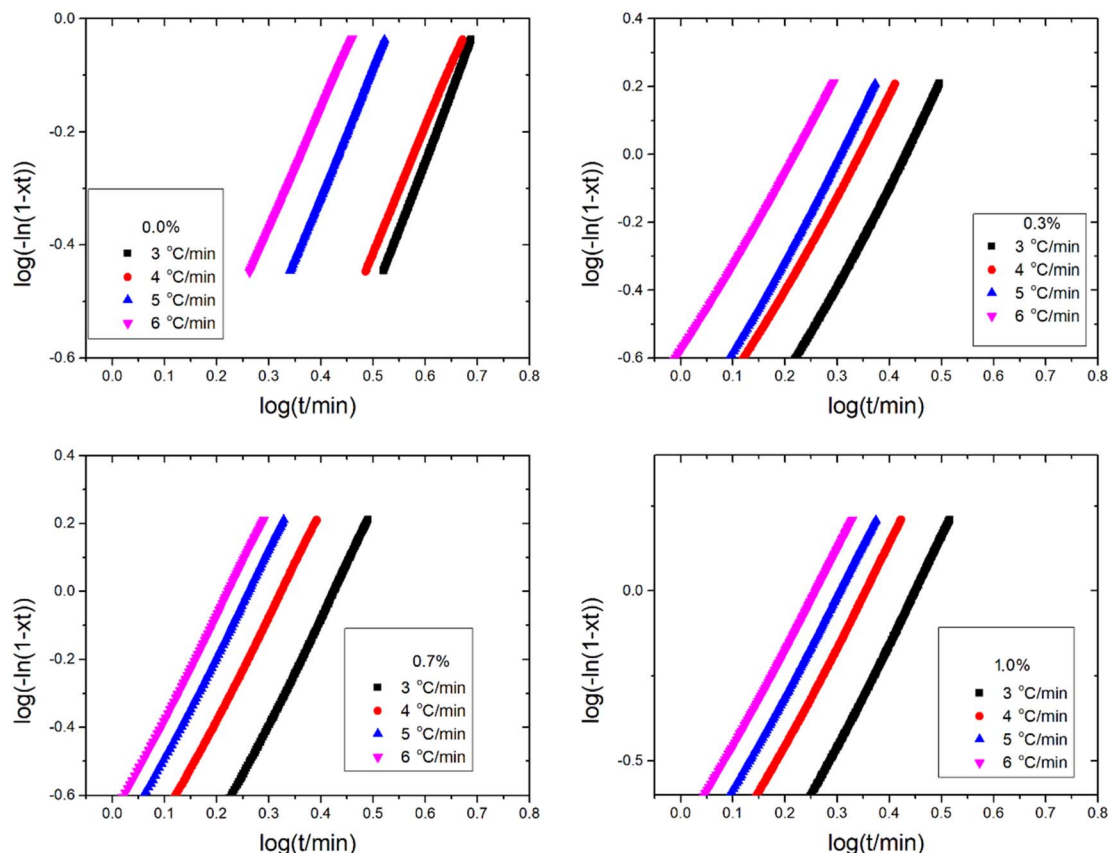
Fig. 9 Modified Avrami plots for PLLA and PLLA–BDOBH samples at various heating rates.

crystallization due to agglomeration of BDOBH particles, as seen in Fig. 4.

3.7 MO model

To characterize the non-isothermal crystallization process, Mo and his colleagues[58] devised a method that combines the Avrami and Ozawa models. This method is expressed as follows:

$$\log(\varnothing) = \log(F(T)) - \alpha \log(t) \tag{6}$$

The plots of $\log(\varnothing)$ *vs.* $\log(t)$ at various conversions of the plain PLLA and PLLA-BDOBH samples are shown in Fig. 10. The associated $F(T)$ and α values are provided in Table 4. The observations of significant linear correlations between $\log(\varnothing)$ and $\log(t)$ for all studied samples suggest that Mo's model effectively describes the non-isothermal crystallization of the PLLA-BDOBH, as indicated by the values of linear regression R^2. Higher $F(T)$ values indicate more crystallization process complexity $F(T)$ increased with an increase in relative crystallinity in all studied samples. For a given conversion (*i.e.*, 0.6), the order of $F(T)$ values for PLLA-BDOBH samples is PLLA > PLLA-BDOBH-3.0 > PLLA-BDOBH-1.0 > PLLA-BDOBH-0.3 > PLLA-BDOBH-0.7 in consistent with modified Avrami results. At higher concentrations, BDOBH particles may agglomerate, disrupting the uniform nucleation process and introducing kinetic constraints. This leads to an increase in the so-called

"crystallization process complexity," reflected by higher $F(T)$ values. This result also emphasizes that BDOBH, in the range from 0.3 to 1%, fastened the PLLA's crystallization rate. The values of α for all studied samples are constant, as shown in Table 4.

3.8 Activation energy

The Kissinger–Akahira–Sunose (KAS) method[59–61] (eqn (7)) is the approach widely employed for computing the activation energy of nonisothermal cold crystallization.[53] This model suggests that the activation energy, E, varies systematically during the transformation process.

$$\ln\left(\frac{\Phi_i}{T_{\alpha i}{}^2}\right) = C_K(\alpha) - \frac{E_\alpha}{RT_{\alpha i}}, \tag{7}$$

$$C_K(\alpha) = \ln\left[\left|\frac{df(\alpha)}{d\alpha}\right| \frac{A \times R}{E_\alpha}\right]. \tag{8}$$

where t is the time, T is the temperature, α is the relative degree of crystallinity, A (s^{-1}) is the pre-exponential (frequency) factor, E (kJ mol^{-1}) is the activation energy, R is the universal gas constant, and $f(\alpha)$ is the reaction model.

For each degree of the conversion fraction, α, on a conversion range of $\alpha = 0.1$ to 0.9, a corresponding $T_{\alpha i}$ and heating rate are used to plot $\ln\left(\frac{\Phi_i}{T_{\alpha i}{}^2}\right)$ against $\frac{1}{T_{\alpha i}}$. E_α is derived from the
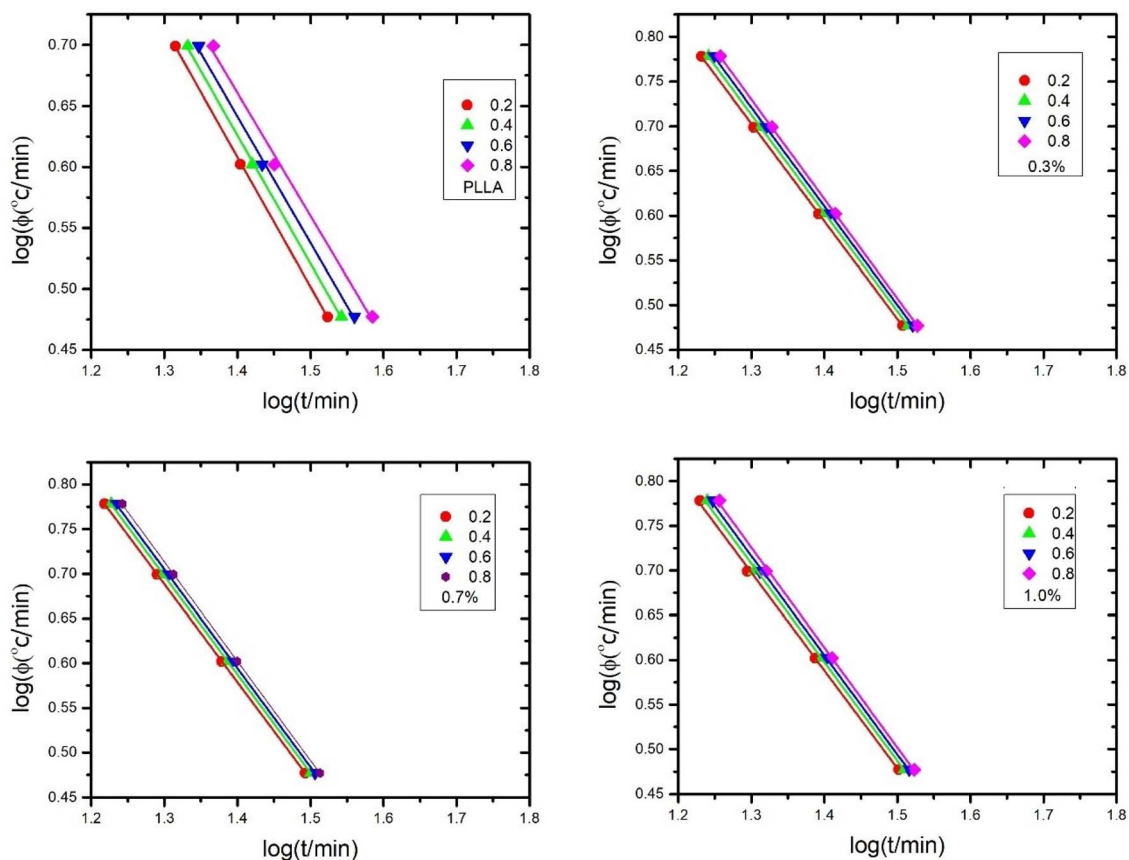
Fig. 10 Plots of $\log(\varnothing)$ as a function of $\log(t)$ for plain PLLA and PLLA/BDOBH samples.

Table 4 $F(T)$ and α values of Mo approach for PLLA/BDOBH

BDOBH (wt%)	Kinetics parameter	$X(t)$			
		0.2	0.4	0.6	0.8
0.0	$F(T)$	154	161	168	176
	b	1.1	1.1	1.2	1.2
	R^2	0.97	0.99	0.99	0.99
0.3	$F(T)$	133	139	144	151
	b	1.1	1.1	1.1	1.1
	R^2	0.999	0.999	0.999	0.999
0.7	$F(T)$	130	135	139	144
	b	1.1	1.1	1.1	1.1
	R^2	0.999	0.999	0.999	0.999
1.0	$F(T)$	133	140	145	152
	b	1.2	1.2	1.2	1.2
	R^2	0.999	0.999	0.999	0.999
3.0	$F(T)$	139	146	158	180
	b	1.1	1.1	1.1	1.1
	R^2	0.999	0.999	0.999	0.999

slope, with regression $R^2 = 0.999$. Fig. 11 shows the dependence of E_α on the conversion, α, and T. The values of Eα are positive and show a decrease with an increase in α, as shown in Fig. 11a. A combination of nucleation and growth rate determines the overall crystallization rate. Since the activation energies of these

two mechanisms are probably different, the effective activation energy will vary with temperature. Vyazovkin and Dranca[62] reported that the effective activation energy values decreased as the crystallization temperature increased within the studied crystallization range situated above the glass transition temperature but below the maximum crystallization rate. Therefore, the values of effective activation energy of PLLA and PLLA-BDOBH decreased with an increase in temperature, as shown in Fig. 11b. The order of E_α is in good agreement with the values of the observed cold crystallization peaks, as shown in Fig. 11 and Table 3. All results indicate that crystallization of PLLA occurs at lower temperatures in the presence of BDOBH. E_α decreases substantially with α. This aligns with the fact that as the conversion α increases, the temperature shifts to a higher value during a heating run from a glassy state. At lower temperatures (or earlier stages of crystallization), the presence of 3 wt% BDOBH may still provide sufficient nucleation sites, slightly promoting crystallization (Fig. 10). However, as crystallization progresses or at higher temperatures, the effect of particle agglomeration or restricted chain mobility becomes more pronounced, potentially hindering crystal growth. This transition could result in a change in the dominant crystallization mechanism, as reflected by the change in the slope of activation energy.
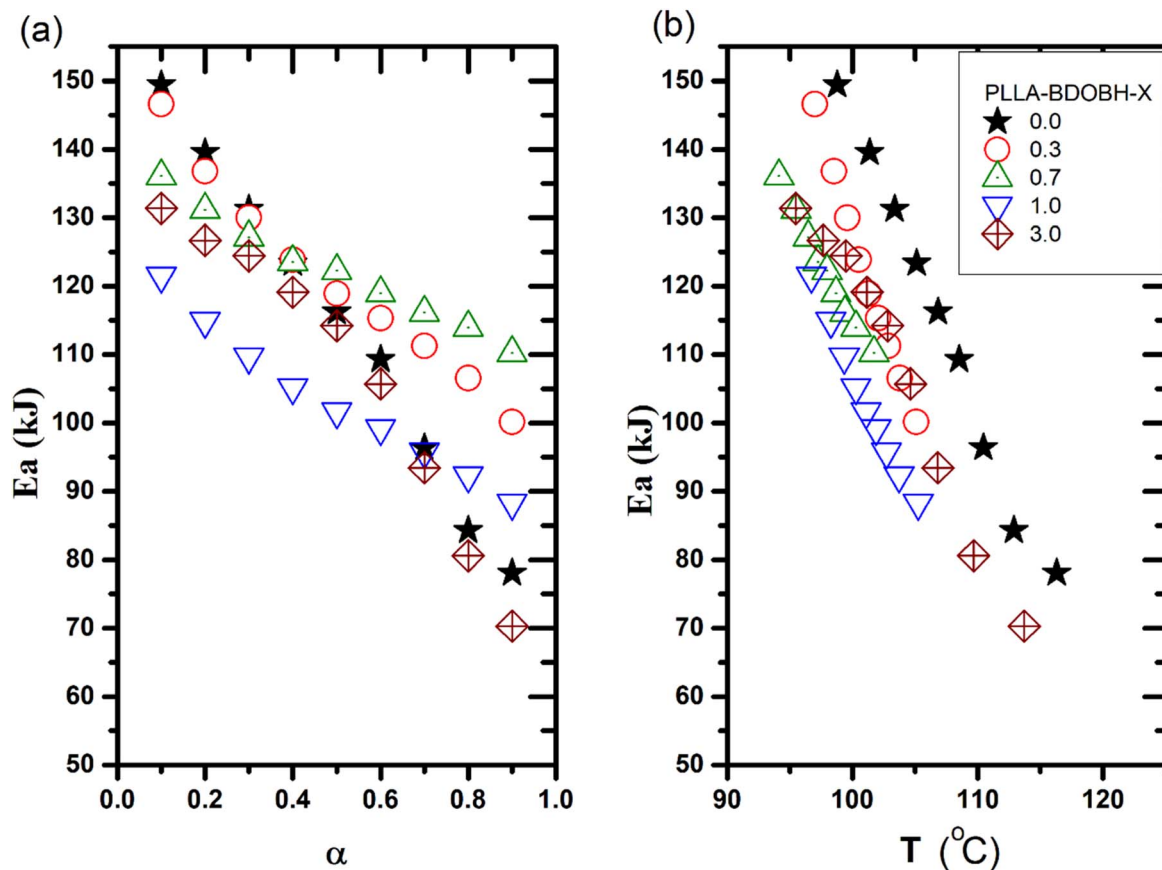
Fig. 11 An effective activation energy as a function of (a) conversion, α and (b) average crystallization temperature.

A similar pattern has been observed in PLLA/PHO/talc.,[56] PLLA/EVA80/TiO$_2$,[8] PLLA/Zn-MOF,[35] and PLLA/metal oxide nanofiller.[63]

4. Conclusion

For the first time, the organic compound 2,2′-(butane-1,4-diylbis(oxy))di(benzohydrazide) (BDOBH) was incorporated into the PLLA matrix to assess its impact on the performance of PLLA. FTIR analysis shows the presence of hydrogen bonds between PLLA and BDOBH. Polarized optical micrographs and DSC experiments demonstrated that BDOBH in a low concentration range from 0.3 to 0.7 wt% acted as an effective nucleating agent, providing sites for heterogeneous nucleation and accelerating the crystallization process of PLLA. The addition of BDOBH led to a significant increase in PLLA's crystallinity, from 12% to 55–60%, a drastic acceleration in the overall crystallization rate, and an increase in thermal stability. Polarized optical micrographs showed a significant increase in the number of PLLA spherulites and a dramatic decrease in the size of PLLA spherulites, without causing any significant change to its crystalline structure. The modified Avrami and Mo models described the cold crystallization kinetics at different heating rates. The activation energy of both neat PLLA and the PLLA-BDOBH blend was determined using the KAS method, demonstrating that adding BDOBH reduced the activation

energy of the PLLA matrix. In summary, incorporating BDOBH as a novel nucleating agent into PLLA significantly improves its crystallization behavior, which expands its potential applications across diverse sectors.

Data availability

Data is available in main text.

Author contributions

Safaa El-Taweel: formal analysis, funding acquisition, methodology, data curation, conceptualization, validation, project administration, resources, software, writing – original draft, writing – review & editing. Sherif M. H. Sanad: methodology, formal analysis, data curation, resources, review & editing. Ahmed E. M. Mekky: methodology, data curation, resources, formal analysis, review & editing.

Conflicts of interest

The authors declare that there is no conflict of interest regarding the publication of this paper.

References

1 A. D. Tripathi, K. Khosravi Darani, D. C. Rai and V. Paul, *Biodegradable Polymer-Based Food Packaging*, Springer Nature Singapore, Singapore, 2022.

2 V. Siracusa, P. Rocculi, S. Romani and M. D. Rosa, *Trends Food Sci. Technol.*, 2008, **19**, 634–643.

3 M. del R. Herrera-Rivera, S. P. Torres-Arellanes, C. I. Cortés-Martínez, D. C. Navarro-Ibarra, L. Hernández-Sánchez, F. Solis-Pomar, E. Pérez-Tijerina and R. Román-Doval, *RSC Adv.*, 2024, **14**, 21832–21858.

4 T. Ageyeva, J. G. Kovács and T. Tábi, *J. Therm. Anal. Calorim.*, 2022, **147**, 8199–8211.

5 T. Tábi, T. Ageyeva and J. G. Kovács, *Mater. Today Commun.*, 2022, **32**, 103936.

6 Z. Refaa, M. Boutaous, S. Xin and D. A. Siginer, *J. Therm. Anal. Calorim.*, 2017, **128**, 687–698.

7 C. Deetuam, C. Samthong, S. Choksriwichit and A. Somwangthanaroj, *Iran. Polym. J.*, 2020, **29**, 103–116.

8 S. H. El-Taweel, *Sci. Rep.*, 2024, **14**, 18142.

9 K. P. Crešnar, L. F. Zemljič, L. Papadopoulos, Z. Terzopoulou, A. Zamboulis, P. A. Klonos, D. N. Bikiaris, A. Kyritsis and P. Pissis, *Mater. Today Commun.*, 2021, **27**, 102192.

10 W. Yu, L. Sisi, Y. Haiyan and L. Jie, *R. Soc. Chem.*, 2020, **10**, 15328.

11 H. Xu, Z. X. Feng, L. Xie and M. Hakkarainen, *ACS Sustainable Chem. Eng.*, 2016, **4**, 334–349.

12 S. W. Kim and H. M. Choi, *Korean J. Chem. Eng.*, 2016, **33**, 330–336.

13 I. M. De Arenaza, J. R. Sarasua, H. Amestoy, N. Lopez-Rodriguez, E. Zuza, E. Meaurio, F. Meyer, J. I. Santos, J. M. Raquez and P. Dubois, *J. Appl. Polym. Sci.*, 2013, **130**, 4327–4337.

14 S. Azizi, M. Azizi and M. Sabetzadeh, *J. Compos. Sci.*, 2019, **3**, 1–15.

15 X. Zhao, J. Yu, X. Liang, Z. Huang, J. Li and S. Peng, *Int. J. Biol. Macromol.*, 2023, **233**, 123581.

16 M. Hajibeygi, S. Faramarzinia, M. Shabanian, S. Norouzbahari and J. Meier-Haack, *Mater. Chem. Phys.*, 2022, **289**, 126497.

17 L. Zhao and Y. Cai, *Emerging Mater. Res.*, 2020, **9**, 1–9.

18 H. Nakajima, M. Takahashi and Y. Kimura, *Macromol. Mater. Eng.*, 2010, **295**, 460–468.

19 J. Li, D. Chen, B. Gui, M. Gu and J. Ren, *Polym. Bull.*, 2011, **67**, 775–791.

20 H. Bai, W. Zhang, H. Deng, Q. Zhang and Q. Fu, *Macromolecules*, 2011, **44**, 1233–1237.

21 P. Song, Z. Wei, J. Liang, G. Chen and W. Zhang, *Polym. Eng. Sci.*, 2012, **52**, 1058–1068.

22 T. Xu, Y. Wang, Q. Han, D. He, Q. Li and C. Shen, *J. Macromol. Sci., Part B: Phys.*, 2014, **53**, 1680–1694.

23 T. Xu, A. Zhang, Y. Zhao, Z. Han and L. Xue, *Polym. Test.*, 2015, **45**, 101–106.

24 Q. Xing, R. Li, X. Dong, F. Luo, X. Kuang, D. Wang and L. Zhang, *Macromol. Chem. Phys.*, 2015, **216**, 1134–1145.

25 L. S. Zhao, Y. H. Cai and H. L. Liu, *Polym. Plastics Technol. Mater.*, 2020, **59**, 117–129.

26 Q. Xing, Z. Wang, R. Li, X. Dong and D. Wang, *RSC Adv.*, 2016, **6**, 113377–113389.

27 N. Kawamoto, A. Sakai, T. Horikoshi, T. Urushihara and E. Tobita, *J. Appl. Polym. Sci.*, 2007, **103**, 198–203.

28 Y. Li and W. Zhen, *Polym. Adv. Technol.*, 2017, **28**, 1617–1628.

29 Z. Zhen, Q. Xing, R. Li and X. Dong, *Thermochim. Acta*, 2020, **683**, 178447.

30 T. Khwanpipat, M. Seadan and S. Suttiruengwong, *Materials*, 2018, **11**, 1139.

31 Y.-H. Cai, L.-L. Tian and Y. Tang, *Polimery*, 2017, **62**, 734–742.

32 Y. H. Cai and S. J. Li, *Eur. J. Chem.*, 2012, **9**, 545–552.

33 P. Ma, Y. Xu, T. Shen, W. Dong, M. Chen and P. J. Lemstra, *Eur. Polym. J.*, 2015, **70**, 400–411.

34 A. E. M. Mekky, S. M. H. Sanad and A. M. Abdelfattah, *Mendeleev Commun.*, 2022, **32**, 612–614.

35 S. H. El-Taweel, S. S. Hassan and K. M. Ismail, *Int. J. Biol. Macromol.*, 2024, **271**, 132691.

36 P. Liu and W. Zhen, *Polym. Adv. Technol.*, 2018, **29**, 2192–2203.

37 Y. Fan, S. Yan and J. Yin, *J. Appl. Polym. Sci.*, 2019, **136**, 1–11.

38 S. H. El-Taweel, O. Alhaddad, M. H. Darweesh and G. R. Saad, *Polym. Adv. Technol.*, 2025, **36**, 28–30.

39 Y. H. Cai, L. L. Tian, L. S. Zhao and M. X. Zhang, *Mater. Res. Express*, 2017, **4**, 105307.

40 Y. H. Cai and Y. H. Zhang, *Adv. Mater. Sci. Eng.*, 2014, **2014**, 1–8.

41 L.-S. Zhao, J. Qiao, W. Chen and Y. Cai, *Polimery*, 2021, **66**, 234–244.

42 J. R. Rocca-Smith, A. Lagorce-Tachon, C. Iaconelli, J. P. Bellat, E. Marcuzzo, A. Sensidoni, F. Piasente, F. Debeaufort and T. Karbowiak, *Express Polym. Lett.*, 2019, **13**, 825–834.

43 H. Yuan, Z. Liu and J. Ren, *Polym. Eng. Sci.*, 2009, **49**, 1004–1012.

44 C. Gao, P. Chen, Y. Ma, L. Sun, Y. Yan, Y. Ding and L. Sun, *Int. J. Biol. Macromol.*, 2023, **253**, 126494.

45 S. Molinaro, M. Cruz Romero, M. Boaro, A. Sensidoni, C. Lagazio, M. Morris and J. Kerry, *J. Food Eng.*, 2013, **117**, 113–123.

46 D. Garlotta, *J. Polym. Environ.*, 2001, **9**, 63–84.

47 W. Wang, A. Saperdi, A. Dodero, M. Castellano, A. J. Müller, X. Dong, D. Wang and D. Cavallo, *Cryst. Growth Des.*, 2021, **21**, 5880–5888.

48 H. Zhang, S. Wang, S. Zhang, R. Ma, Y. Wang, W. Cao, C. Liu and C. Shen, *Polym. Test.*, 2017, **64**, 12–19.

49 X. Dai, Y. Cao, X. Shi and X. Wang, *RSC Adv.*, 2016, **6**, 71461–71471.

50 C. Li and Q. Dou, *Thermochim. Acta*, 2014, **594**, 31–38.

51 A. Jeziorny, *Polymer*, 1978, **19**, 1142–1144.

52 S. H. El-Taweel and M. Abboudi, *J. Appl. Polym. Sci.*, 2020, **137**, 48340.

53 O. Alhaddad, S. H. El-Taweel and Y. Elbahloul, *Open Chem.*, 2019, **17**, 1266–1278.

54 S. H. El-Taweel and A. Al-Ahmadi, *J. Therm. Anal. Calorim.*, 2019, **137**, 1657–1672.

55 S. H. El-Taweel, A. O. Al-Ahmadi, O. Alhaddad and R. M. Okasha, *Molecules*, 2018, **23**, 2703.

56 S. H. El-Taweel and A. Al-Hamdi, *J. Therm. Anal. Calorim.*, 2024, **149**, 1351–1364.

57 W. Phetwarotai and D. Aht-Ong, *J. Therm. Anal. Calorim.*, 2017, **127**, 2367–2381.

58 T. Liu, Z. Mo, S. Wang and H. Zhang, *Polym. Eng. Sci.*, 1997, **37**, 568–575.

59 M. J. Starink, *Thermochim. Acta*, 2003, **404**, 163–176.

60 H. E. Kissinger, *Anal. Chem.*, 1957, **29**, 1702–1706.

61 Z. Zhang, J. Chen, H. Liu and C. Xiao, *J. Therm. Anal. Calorim.*, 2014, **117**, 783–787.

62 S. Vyazovkin and I. Dranca, *Macromol. Chem. Phys.*, 2006, **207**, 20–25.

63 E. Tarani, K. Pušnik Črešnar, L. F. Zemljič, K. Chrissafis, G. Z. Papageorgiou, D. Lambropoulou, A. Zamboulis, D. N. Bikiaris and Z. Terzopoulou, *Appl. Sci.*, 2021, **11**, 3004.